Hindawi
Shock and Vibration
Volume 2020, Article ID 9786182, 11 pages
https://doi.org/10.1155/2020/9786182

Research Article

Numerical Simulation of Fluid-Solid Coupling in Surrounding Rock for River Stope Mining

Haiping Yuan,[1,2] Chenghao Chen,[1] Zhongming He,[2] and Yixian Wang[1]

[1]*School of Civil and Hydraulic Engineering, HeFei University of Technology, Hefei, China*
[2]*State Engineering Laboratory of Highway Maintenance Technology, Changsha University of Science & Technology, Changsha, China*

Correspondence should be addressed to Yixian Wang; wangyixian2012@hfut.edu.cn

Received 14 January 2020; Accepted 10 April 2020; Published 29 April 2020

Academic Editor: Anil Kumar

Mining disturbance will induce further weakening of faults and rock bridges, improve rock mass permeability and, in serious cases, conduct surface rivers to cause disasters. A numerical calculation model of river-fault in the mining area is established. Based on the fluid-solid coupling theory of rock mass, the influence of mining disturbance on the development and evolution process of rock bridge rupture and river-fault-stope potential seepage channel is simulated and calculated. Research studies show that under the disturbance of ore body mining, it is possible to form a channel from the river to fault to seepage and drainage in the stope. The disturbance of ore body mining has no great adverse effect on the stability of the rock mass at the top of F2 fault. The rock mass damage caused by mining is only distributed in local areas, and the rock bridge between the river, fault, and stope is not completely connected. The fracture of mining rock mass leads to the increase in permeability of rock mass, and seepage tends to spread in the direction of the fault, but there is no obvious through drainage channel from surface water to the stope. The results of research provide technical guidance for the mine to use the filling mining method after the river does not change the road safety and reliability certification and can also provide reference for similar mines.

1. Introduction

Under the actions of tectonic movement, weathering, erosion, etc, a natural geological body develops a large number of fissures or even faults with different directions and sizes which are cutting each other. The existence of these joints and faults provides necessary channels for the infiltration and flow of surface water and groundwater. Mining has a nonnegligible disturbance to the fault. When the rock mass is disturbed by mining unloading, the original stress balance state of the surrounding rock mass is destroyed, which promotes further development of fractures, thus leading to changes in the permeability of the surrounding rock and the flow state of groundwater. When the rock bridge between the fault and the stope is seriously damaged, it results in the development of fractures through and affects the underground aquifer or surface water, and the water will flow into the stope, causing water inrush and mud inrush disasters [1–5].

At present, scholars generally use fluid-solid coupling theory to study the effect of water on disturbed rock mass. Based on the classical Biot seepage mechanics and the split evolution model of the curve expansion path, scholars such as Yang et al. [6] and Nie et al. [7], respectively, studied the rock crack growth and failure mechanism under the action of pore water pressure. Zhang et al. [8], Li et al. [9], Lu [10], and others analyzed the coupling evolution process of the stress field, seepage field, and damage field of rock mass and studied the coupling mechanism of stress-seepage-damage during the formation of the water inrush passage. Bai [11], Yao and Lu [12], Park and Wang [13], and Zoback and Byerlee [14] found that the rock permeability coefficient is changing after being disturbed; Zhu and Wei [15], Zhao and Peng [16], and other scholars put forward the fluid-solid coupling prediction model of disturbed rock mass under the influence of karst geomorphology and the water inrush prevention mechanism under the corresponding conditions.

In conclusion, the research studies on seepage disturbed rock mass by scholars mainly focus on the mechanism of rock crack propagation and the seepage model of rock mass. There are few reports on the fracture mechanism, damage effect, and seepage channel formation of the stope-fault rock bridge under complex conditions of fault influence and mining disturbance.

Based on the engineering background of the influence of the Xima River on the seepage of the filling mining method in the Makeng Iron Mine, this paper establishes a fluid-solid coupling numerical analysis model of ore body mining based on FLAC^{3D}, studies the damage effect of the fault-stope-rock bridge and the dynamic response of the seepage channel after mining disturbance, demonstrates the safety and reliability of the river (Xima River) in the mining area without diversion, and provides reference for similar mining projects. The method described in this article relies on the actual situation of the project to dynamically and iteratively calculate the seepage parameters and deformation data. The cloud image of the parameters related to the rock bridge breaks intuitively reflecting the disruptive effects of mining disturbances and provides theoretical support for the safety assessment of mining activities under rivers.

2. Rock Bridge Fracture Fluid-Solid Coupling Technology

2.1. Fracture Mode of Mining-Induced Rock Bridge. At the same time, the rock mass containing joints, weak planes, and faults is further weakened under mining disturbance such as large-scale blasting, which easily causes damage or even breaks the rock bridges between stopes and faults. At present, the research on the rock bridge is mainly based on the Lajtai rock bridge failure theory [17–19], which holds that with the change of normal stress, rock bridge failure modes are divided into three types: tensile failure, shear failure, and tensile shear composite failure [20]. As shown in Figure 1, the typical pure shear and tensile shear failure modes of rock bridges obtained from uniaxial compression tests are presented.

For the problem of ore body mining, the failure mode of the rock is mainly shear failure and tensile shear failure within the stress range of most mining surrounding rock. The main formula is shown in equation (1), whereτ_{L} is the shear strength, c is the cohesion of the rock,φ is the angle of internal friction, and σ_{n} is the normal stress:

$$\tau_L = \left[\frac{(2c + \sigma_n \tan\varphi)^2}{1 + \tan^2\varphi} - \sigma_n^2\right]^{1/2}. \quad (1)$$

Based on equation (1), the software is developed again through the FISH language embedded in FLAC^{3D}, and codes are written to simulate the fracture of the mining rock bridge.

2.2. Principle of Fluid-Solid Coupling in Mining. When simulating the fluid-solid coupling mechanism of rock mass, the rock mass is regarded as a porous medium [12] and the fluid-solid coupling calculation is carried out taking into account both fluid and mechanical effects. The fluid-solid coupling process includes two mechanical effects: on the one hand, groundwater seepage in rock mass will produce seepage volume force, thus changing the original stress state of rock mass; on the other hand, changes in the stress state of the rock mass will lead to deformation of the rock mass. Changes in the structure of the rock mass will affect the permeability of the rock mass, and then the flow state of water in the rock mass will also change [22]. The calculation flow of fluid-solid coupling is shown in Figure 2.

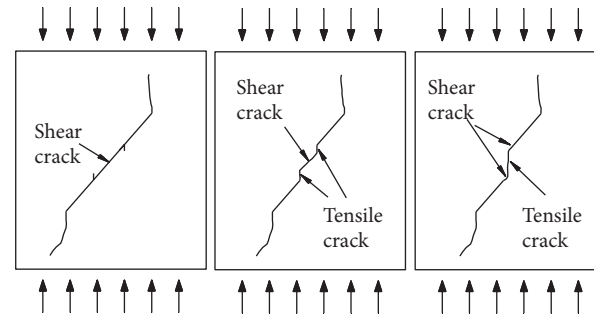

Figure 1: Shear failure and tensile shear failure of the rock bridge [21].

The permeability of rock mass is a process closely related to the initiation, propagation, coalescence, and mesodamage evolution of macrocracks. The relationship between volumetric strain and permeability of rock mass is approximately an exponential function, which can better reflect the evolution law of overall permeability during the rock damage process, as shown in equation (2) [23]. In the equation, k is the permeability coefficient, p is the pore water pressure,ξ is the permeability jump coefficient, β is the coupling coefficient,σ_{ii} is the average stress, H is the Biot constant, and a is the pore water pressure coefficient:

$$k(\sigma, p) = \xi k_0 e^{-\beta\left(\frac{\sigma_{ii}/3 - ap}{H}\right)}. \quad (2)$$

Before the group crack initiation or propagation, the stress-seepage coupling effect of the rock bridge fracture channel and its adjacent rock mass is not obvious, but with the continuous action of mining disturbance and groundwater pressure, new damage points appear continuously and the stress-seepage-damage coupling effect becomes extremely obvious. In order to fully reflect the sharp increase of the permeability coefficient after rock mass damage, it can be regarded as an elasto-brittle material with residual strength and its stress-damage field evolution law during loading and unloading process conforms to the elastic damage theory. The Mohr–Coulomb criterion and the maximum tensile strength criterion were used as damage thresholds for damage identification of elements [24]: when the element reaches the damage threshold of tensile strength f_t, the damage variable D is shown in equation (3a) and the permeability coefficient k of the corresponding element is shown in equation (3b); when the shear stress of the element reaches the damage threshold, the damage variable D is shown in equation (3c) and the permeability coefficient k of the corresponding element is shown in equation (3d):

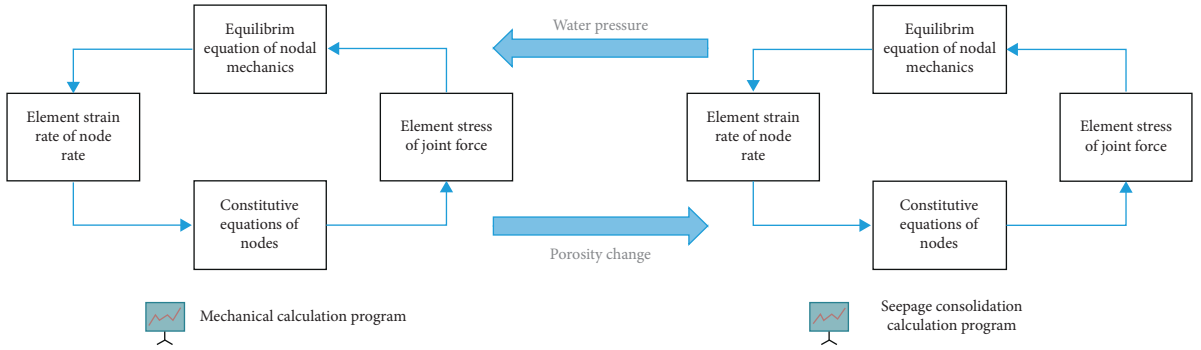

Figure 2: Flowchart of fluid-solid coupling calculation.

$$D = \begin{cases} 0, & \varepsilon_0 \le \varepsilon, \\ 1 - \dfrac{f_{\mathrm{tr}}}{E_0 \varepsilon}, & \varepsilon_{t0} \le \varepsilon < \varepsilon_0, \\ 1, & \varepsilon < \varepsilon_0, \end{cases} \tag{3a}$$

$$k = \begin{cases} k_0 e^{-\beta(\sigma_3 - \alpha p)}, & D = 0, \\ \xi k_0 e^{-\beta(\sigma_3 - \alpha p)}, & 0 < D < 1, \\ \xi' k_0 e^{-\beta(\sigma_3 - p)}, & D = 1, \end{cases} \tag{3b}$$

where f_{tr} is the tensile residual strength and $\xi\prime$ is the increase coefficient of the permeability coefficient when the unit is destroyed.

$$D = \begin{cases} 0, & \varepsilon < \varepsilon_{c0}, \\ 1 - \dfrac{f_{cr}}{E_0 \varepsilon}, & \varepsilon_{c0} < \varepsilon_r, \end{cases} \tag{3c}$$

$$k = \begin{cases} k_0 e^{-\beta(\sigma_1 - \alpha p)}, & D = 0, \\ \xi k_0 e^{-\beta(\sigma_1 - \alpha p)}, & D > 0, \end{cases} \tag{3d}$$

where f_{cr} is the compressive residual strength, ξ_{c0} is the maximum compressive strain, and ξ_r is the residual strain.

2.2.1. Biot Consolidation Theory [25, 26].

$$\left.\begin{aligned} G\nabla^2 u - (\lambda + G)\frac{\partial \varepsilon_v}{\partial x} - \frac{\partial p_w}{\partial x} = 0 \\ G\nabla^2 u - (\lambda + G)\frac{\partial \varepsilon_v}{\partial y} - \frac{\partial p_w}{\partial y} = 0 \\ G\nabla^2 u - (\lambda + G)\frac{\partial \varepsilon_v}{\partial z} - \frac{\partial p_w}{\partial z} = 0 \end{aligned}\right\}, \tag{4a}$$

$$\begin{aligned} &\frac{1}{\gamma_w}\left[k_h\left(\frac{\partial^2 p_w}{\partial x^2} + \frac{\partial^2 p_w}{\partial y^2}\right) + k_v \frac{\partial^2 p_w}{\partial z^2}\right] \\ &\quad = -\frac{\partial \varepsilon_v}{\partial t} = \frac{\partial}{\partial t}\left(\frac{\partial u}{\partial x} + \frac{\partial v}{\partial y} + \frac{\partial w}{\partial z}\right), \end{aligned} \tag{4b}$$

where u, v, and w are the displacement components of the microbody soil skeleton along the positive direction of x, y, and z, respectively; the body strain $\varepsilon_v = \varepsilon_x + \varepsilon_y + \varepsilon_z = -(\partial u/\partial x + \partial v/\partial y + \partial w/\partial z)$, takes compression as positive; E, μ, and G are the elastic modes of soil under drainage conditions, respectively; quantity, Poisson's ratio, shear modulus $G = E/2(1+\mu)$, and Lame constants $\lambda = \mu E/(1+\mu)(1-2\mu)$; the amount of water flowing out of the soil microunit per unit time is equal to the volume change of the microelement, the horizontal permeability coefficient $k_h = k_x = k_y$, and the vertical permeability coefficient $k_v = k_z$; p_w is the pore pressure and γ_w is the severity of water.

2.2.2. Equilibrium Equation.

$$-q_i + q_v = \frac{\partial \xi}{\partial t}, \tag{5}$$

where q_i is the seepage velocity, q_v is the fluid strength of the measured volume, and ξ is the volume change of fluid per unit volume of the porous medium.

2.2.3. Equation of Motion. The motion of the fluid is described by Darcy's law. For the case where the density of homogeneous and isotropic solids and fluids is constant, the equation is

$$q_i = -k\left[p - p_f x_j g_j\right], \tag{6}$$

where k is the permeability coefficient of the medium, p is the pore pressure, p_f is the fluid density, x_j is the distance gradient in 3 directions, and g_j is the three components of gravitational acceleration.

2.2.4. Constitutive Equation. In the case of only considering the effect of stress field and seepage field without considering other external fields such as temperature field, the incremental form of the porous media seepage constitutive equation is as follows:

$$\frac{1}{M}\frac{\partial p}{\partial t} + \frac{n}{s}\frac{\partial s}{\partial t} = \frac{1}{s}\frac{\partial \xi}{\partial t} - \alpha \frac{\partial \varepsilon}{\partial t}, \tag{7}$$

where M is the Biot modulus, n is the fluid density, s is the saturation, ε is the volume strain, and α is the Biot coefficient.

2.2.5. Compatibility Equation. The relationship between the strain rate and the velocity gradient is as follows:

$$\dot{\varepsilon}_{ij} = \frac{1}{2}\left[v_{i,j} + v_{j,i}\right], \tag{8}$$

where $v_{i,j}$ and $v_{j,i}$ are the velocities of a certain point in the medium and i and j represent directions.

In FLAC^{3D}, the software is based on the quasistatic Biot consolidation theory and combines the fluid mass balance equation, Darcy's law, seepage-stress function (equation (2)), and seepage-damage function (equations 3a–3d) to realize fluid-solid coupling calculation under the condition of known volume strain in advance.

3. Spatial Relationship between Engineering Rivers and Faults

3.1. Engineering Survey. A group of tight anticline and syncline folds and fractures accompanying folds are developed in the Makeng Iron Mine area, as shown in Figure 3. The fold trend and the fault strike are mainly distributed in the northeast or north-north direction, controlling the shape and occurrence of the main ore body; in the western part of the ore section, the near-north-trending folds and faults are also well developed; in addition, faults in the northwest direction are poorly developed. The faults in the ore section mainly include NE-trending F1 normal fault, F2 reverse fault, F3 reverse fault, F14 slow fault, NW-trending Ximahe fault, and F20 normal fault.

According to the geological report of the mining area, the spatial relationship of rivers, faults, and ore bodies in the Ximahe mining area is established as shown in Figure 4. The ore body is basically connected to the F2 fault, close to the F20 fault, and far away from the F1 fault, and the F20 fault is located on the upper part of the ore body; in addition, according to the illustration and detailed exploration geological report, the Xima River is theoretically intersected with the F1 fault, the F2 fault, and the F20 fault, that is, the fault itself is a water-filled fault that connects the surface water. Therefore, it is preliminarily believed that if the mining disturbance damage effect is obvious after mining the ore body in the Ximahe mining area, the rock bridge between the stope and the fault may be broken, thus forming the seepage channel of the Ximahe⟶fault⟶stope.

3.2. Model Establishment. According to the topographic geological map of the Makeng area, the average elevation of the Xima River is +450 m, and the main ore body of the mining area is 1600 m long, with a tendency of 490~1300 m. The mining area includes 5 sections of +50 m, +10 m, −50 m, −90 m, and −150 m, and each section is 40 m high, of which −10 m ~ +10 m, and −110 m ~ −90 m are, respectively, middle-level horizontally isolated pillars. Through the extraction and integration of useful information in geological sections and topographic maps, techniques such as triangular patch connection and Boolean operations are used to generate a true three-dimensional model of the geological body that can completely describe the spatial structure, geometry, and spatial boundaries of the rock mass. The main process is shown in Figure 5. Considering the complexity of the model and the accuracy of the calculation results, the calculation model is simplified as a whole, and the faults, pillars, mines, and nearby rock masses are unit encrypted, and a three-dimensional model as shown in Figure 6 is established.

The length, width, and height of the model are 1200 m × 1340 m × 800 m, including 808415 cells and 135000 nodes. At the same time, in order to better study the rock bridge failure process and seepage process, four monitoring points as shown in Figure 7 were set up along the section (the section passes through the center point of the ore body and is perpendicular to the x-axis, hereinafter referred to as section 1). Among them, monitoring points 1 to 3 are located between the F2 hanging wall ore body and F2 fault.

Ore bodies, surrounding rocks, faults, and backfills have different physical and mechanical properties. The calculation parameters of rock physical mechanics are obtained through laboratory tests. In combination with field fracture surveys, the rock mechanical parameters are converted into the rock body mechanical parameters. The seepage parameters are directly derived from field measurements. The physical and mechanical calculation parameters and seepage parameters of the rock body are shown in Table 1 [27–30]. The yield criterion applies the Mohr–Coulomb criterion. The top surface of the model is free, the bottom surface and the periphery are restrained by chain bars, and the stress field is simulated according to the self-weight stress field. The total water head of the initial seepage field of the model is +450 m, the periphery is set as the impermeable boundary, and the mined-out area after ore body mining is set as the drainage boundary and saturated stable seepage is assumed. The vertical stress of rock mass is the weight of rock mass plus confined water pressure.

According to the existing mining plan, the model is mined in the order of +50 m mine section, +10 m mine section, −50 m mine section, −90 m mine section, and −150 m section. The mining steps of each section comprise 4 steps: mining room mining, mine filling, pillar mining, and pillar filling (20 working conditions in total). Based on the above simulation scheme, this paper focuses on the damage effect of the rock bridge in mining and the seepage characteristics of the rock mass at different times when the rock bridge is destroyed the most seriously (i.e., when it is mined to −150 m).

4. Analysis of Fluid-Solid Coupling Numerical Simulation Results

4.1. Fracture Analysis of Rock Bridge in River-Fault-Stope. Figures 8 and 9 show the volumetric curve of the plastic zone in the rock bridge area and the vertical displacement curve of each measuring point with the advancement of mining. It can be seen from the figure that the volume of the plastic zone in the rock bridge area and the vertical displacement of each measuring point were gradually increased after the ore is mined, and the volume of the plastic zone suddenly increased when the mining section 10 m and the mining section −150 m were mined, and the displacement increment was relatively larger, indicating the possibility of large-scale damage to the rock mass during the mining of the two mine sections. At the same time, in the plastic zone volume after 3

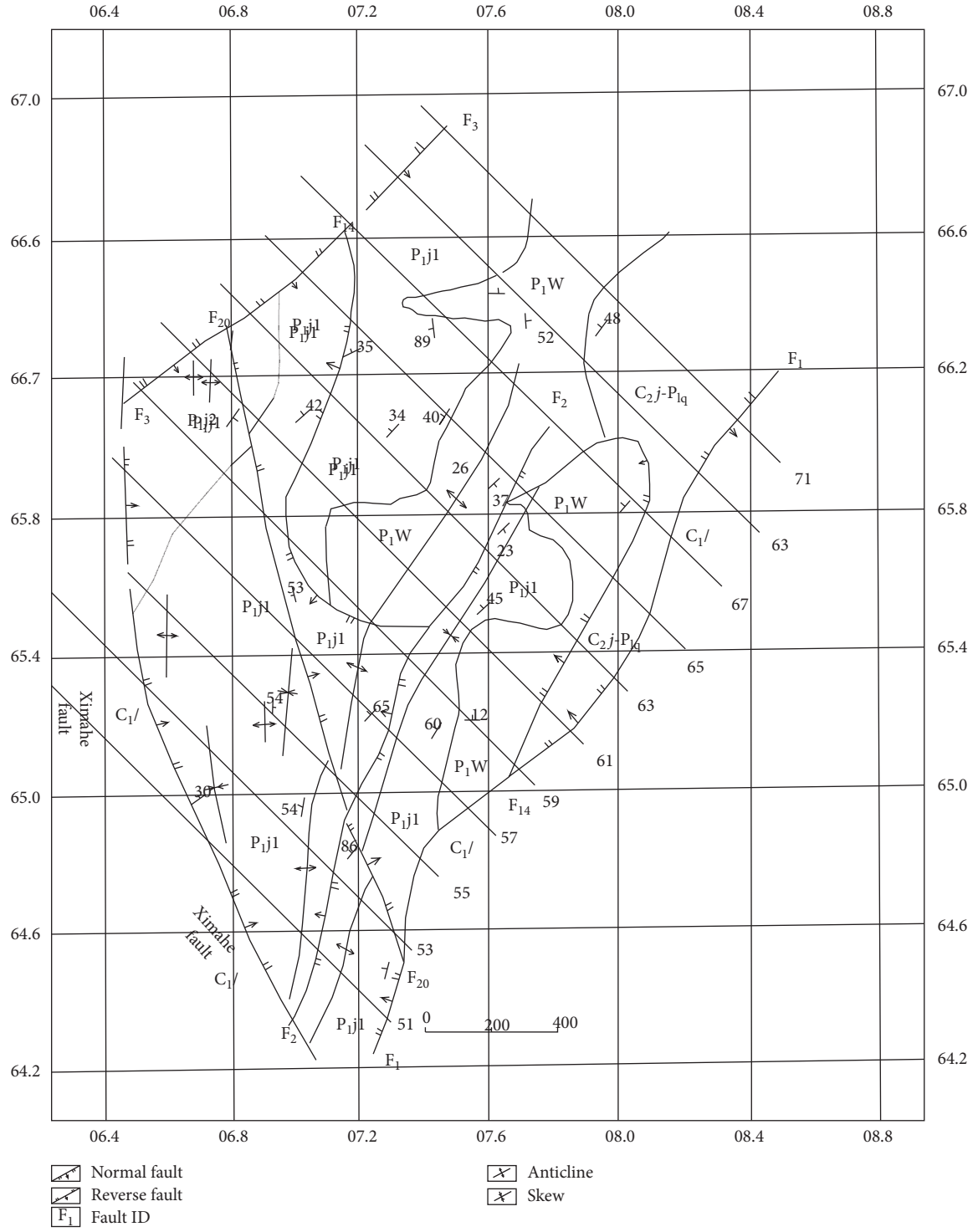

Figure 3: Geological map of the Makeng Iron Mine.

working conditions, the shear failure accounts for more than 80%, which shows that the rock bridge failure is dominated by shear failure.

Section 1 passes through the center of the ore body and is perpendicular to the x-axis, while section 2 passes through the center of the ore body and intersects with faults F2 and F20, with an angle of 60° with section 1, as shown in Figure 10. After the filling and mining of the ore body above the −150 m ore section is completed, it can be seen from the plastic zone distribution diagram (Figure 11) and stress distribution diagram (Figure 12) of section 1 and section 2 that stress release, secondary redistribution of stress field, and local stress concentration occur in the surrounding rock mass of the stope after the ore body is excavated. Due to the existence of F2 and F20 faults and the influence of weak fault strength and close proximity to the fault, cross tensile stress

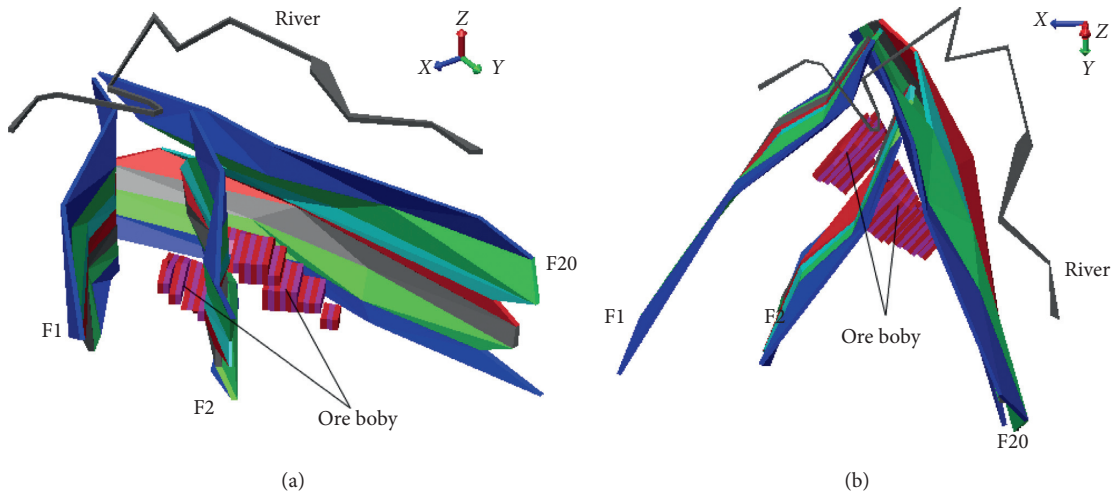

Figure 4: Spatial relation map of rivers, faults, and ore bodies. (a) Perspective one. (b) Perspective two.

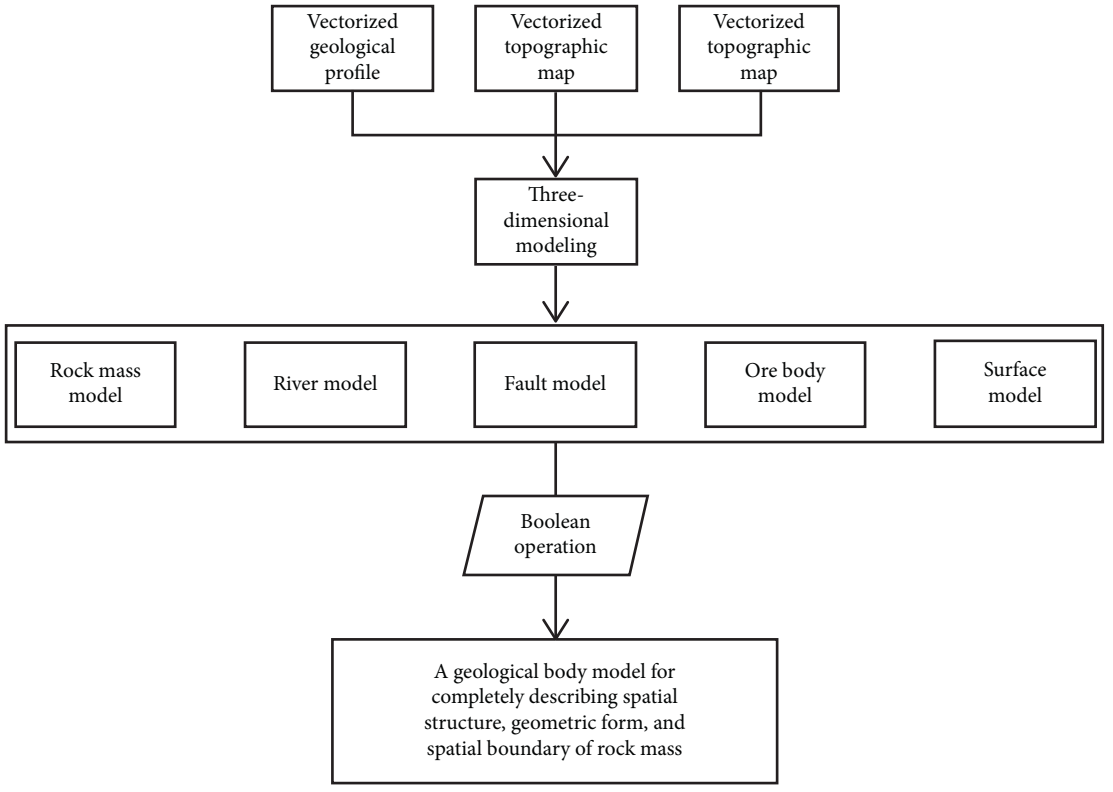

Figure 5: Flowchart of geological body modeling.

distribution zones are formed in the upper wall of F2 upward along the upper right corner of the stope and in the lower wall of F20 upward along the upper left corner of the stope, resulting in obvious tensile shear failure of the rock mass. The plastic failure zone of surrounding rock is mainly distributed in the center of the stope roof, stope corner, rock bridge between fault and stope, weak strength zone of structural fracture zone, and other areas. Although mining has led to the local destruction of stope periphery, faults, rock bridges between faults and stopes, and even to the penetration destruction in very small areas, after the filling and mining of ore bodies above −110 m, the volume of the plastic zone is 1.8 million m^3, accounting for only 8.5% of the total volume of 2127 m^3 of rock bridges, and there is no obvious further destruction of rock masses on the top of faults F2 and F20, which indicates that mining disturbance has not had a great adverse effect on the stability of rock masses on the top of faults F2 and F20. The distribution of rock mass destruction area caused by ore body mining is limited to a local area. From a global perspective, the destruction area does not completely penetrate stope-rock bridge-fault-Xima River.

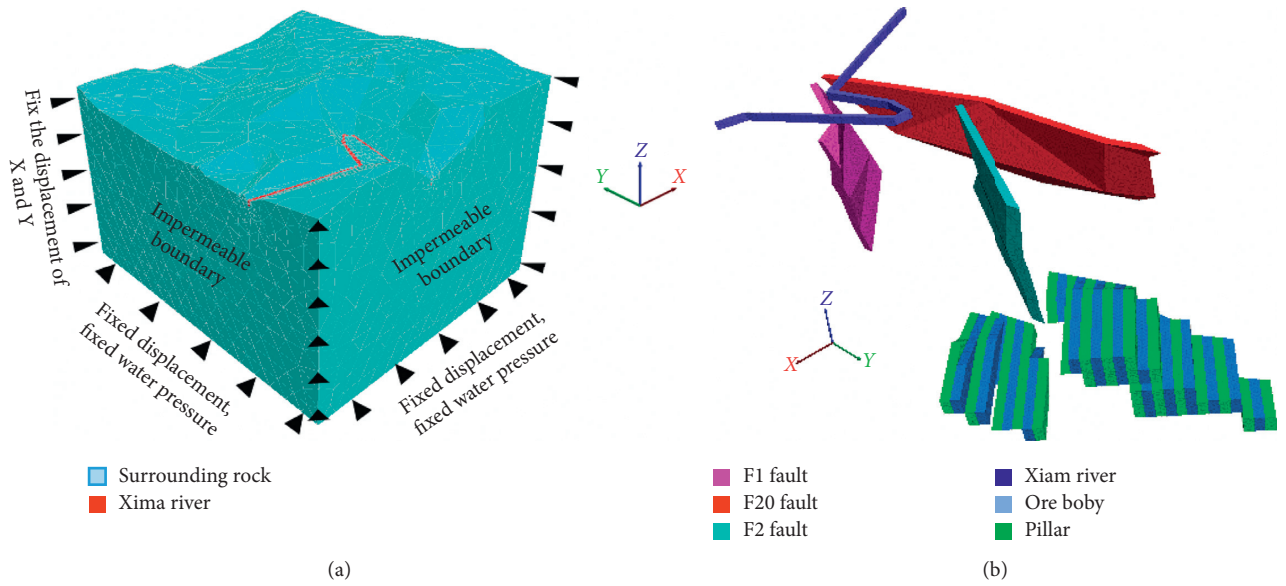

Figure 6: 3D stereoscopic model.

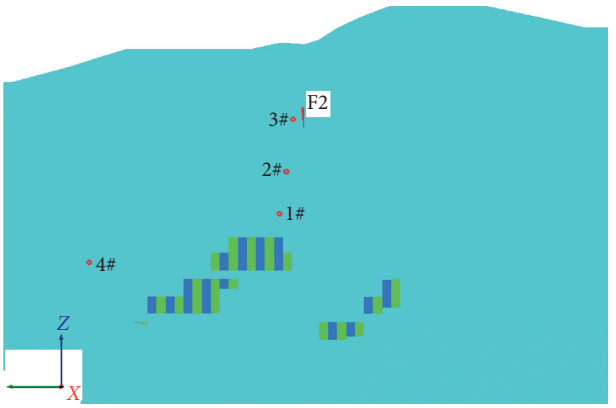

Figure 7: The layout of the monitoring point.

Table 1: Parameters for different rocks mass.

Material science	Density (g·cm^{-3})	Tensile strength (MPa)	Modulus of elasticity (GPa)	Poisson's ratio μ	Cohesive force (MPa)	Internal friction angle f (°)	Seepage coefficient (cm/s)	Fluid modulus (GPa)
Ore rock	3846	2.7	30	0.22	6.5	32	1e-8	1.0
Surrounding rock	2680	1.8	30	0.24	2.5	29	1e-6	1.0
Fault	2300	0.6	0.3	0.3	0.1	28	1e-5	1.0
Backfill	2000	0.8	0.4	0.31	0.1	22	1e-6	1.0

4.2. Analysis of Seepage Capacity of Potential Seepage Channels. The ore mining disturbance will cause the surrounding rock mass to be destroyed, and the permeability of the rock mass will be improved after the rock mass is damaged, as shown in equations (2) and 3a–3d, that is, the rock mass permeability is a function of the stress and the induced damage variable. It can be considered that in the elastic phase, the rock stress and permeability have a negative exponential relationship, and the jump of the permeability is considered to increase after the damage. According to the calculated parameter values of the influencing factors, the permeability coefficient of the plastic

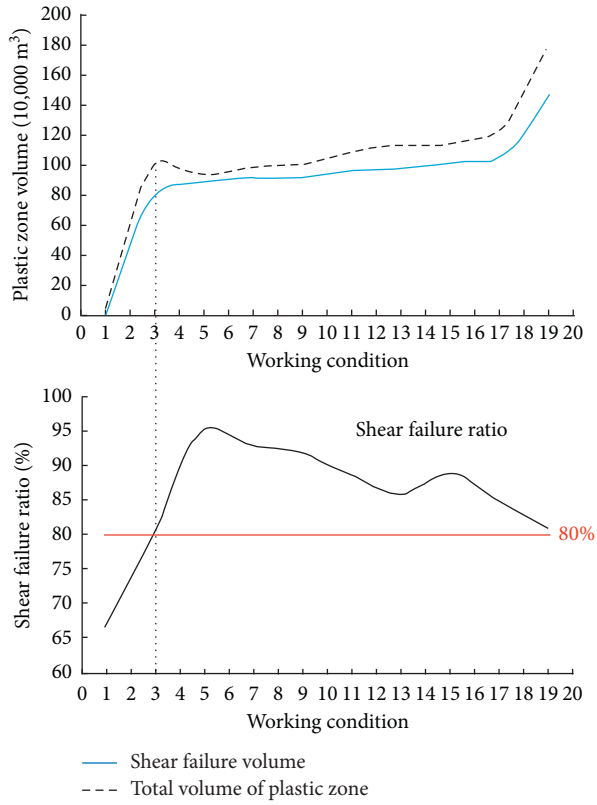

Figure 8: Volume curve of the plastic zone in the rock bridge region.

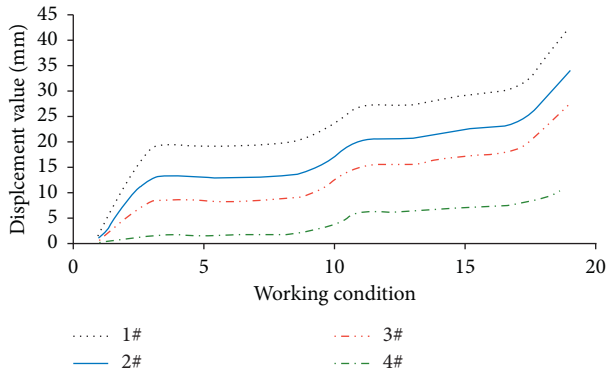

Figure 9: Vertical displacement curve of each measuring point.

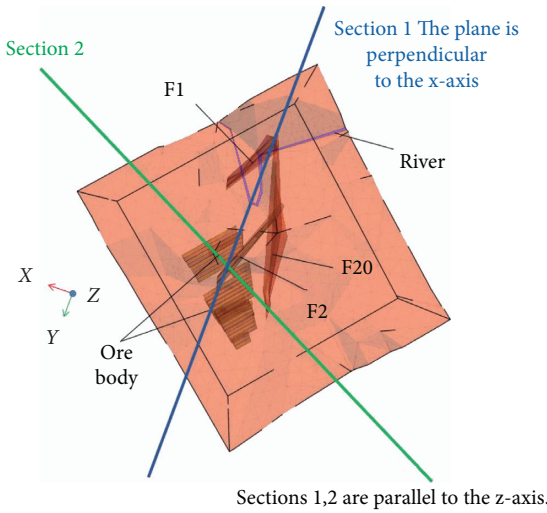

Figure 10: The positions of sections 1 and 2.

failure unit increases when the seepage is calculated. From the relationship curve between pore water pressure and seepage time at each monitoring point (Figure 13), it can be seen that after mining the ore body, the pore water pressure value changes greatly with time within 1~10 days, and after 10 days, the pore water pressure value gradually decreases with time and tends to be stable and basically does not change after 30 days of seepage; the change of pore water pressure at monitoring point 3, i.e., monitoring point at fault F2, is very small, indicating that no seepage channel has been formed through to fault F2.

In addition, through the pore water pressure nephogram of different seepage time (Figure 14), it can be seen that with the development of mining, the fracture water conductivity of the mining rock mass near the stope increases gradually. Influenced by the weaker fault strength and the greater permeability of rock mass caused by rock fragmentation, the pore water pressure isoline of the stope

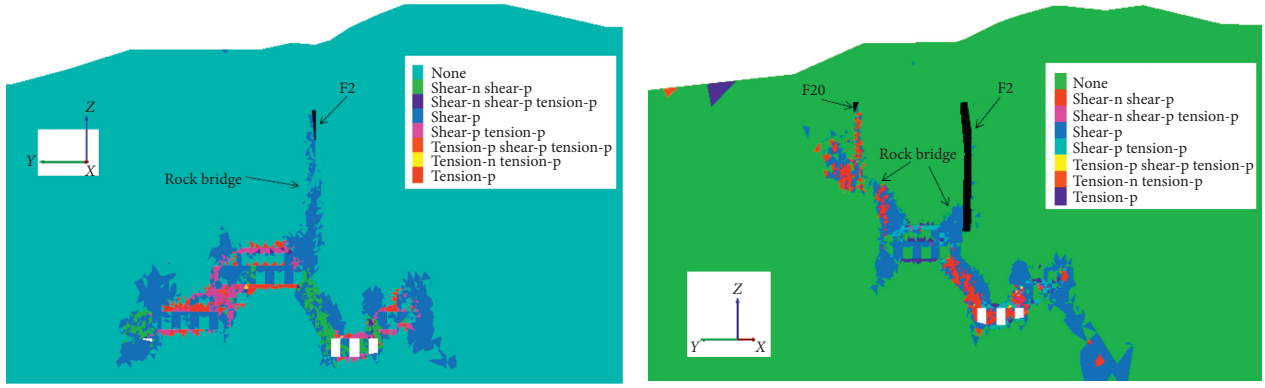

(a) (b)

Figure 11: Plastic zone distribution diagram of model section. (a) Section 1. (b) Section 2.

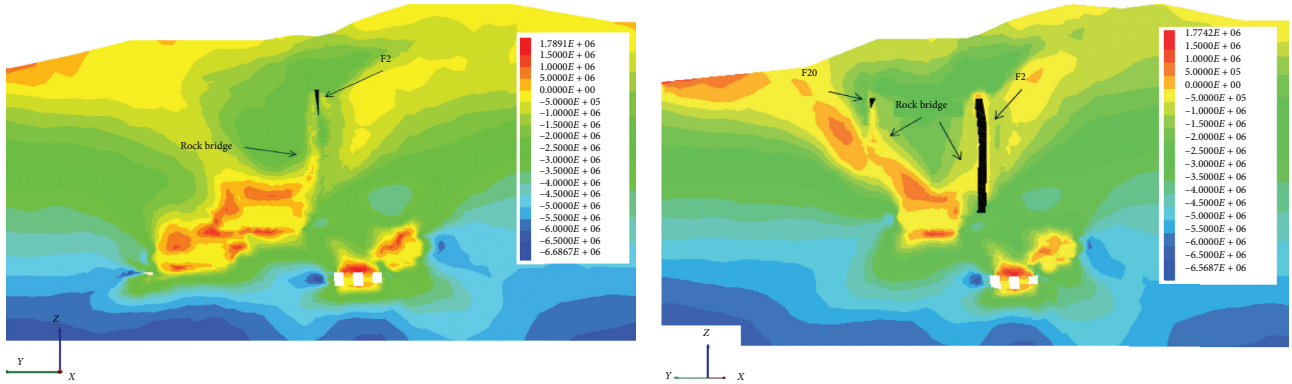

(a) (b)

Figure 12: Stress distribution diagram of model section (Pa). (a) Section 1. (b) Section 2.

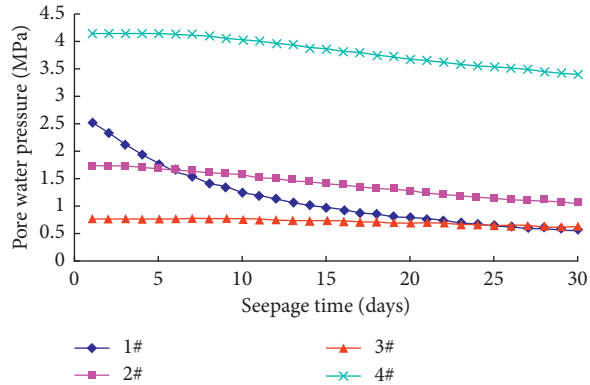

Figure 13: Pore water pressure-seepage time curve at each measuring point.

roof tends to diffuse towards the fault direction with the advance of time, but after 30 days of seepage (that is, after the seepage field is basically stable), the pore water pressure nephogram shows that the seepage field around the stope is not connected with the fault area, that is to say, the seepage field which is obviously connected with the fault is not formed, and the seepage and drainage channel of the river, fault, rock bridge, and stope is not formed.

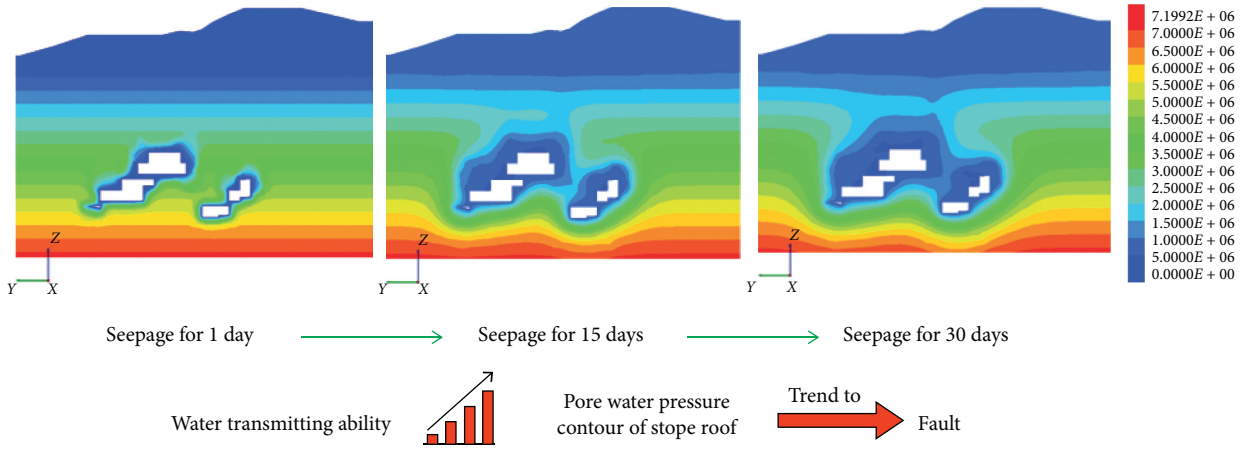

Figure 14: Pore water pressure nephogram (Pa) for different seepage days at section 1 of the model.

5. Conclusion

In this paper, the Flac^{3D} fluid-solid coupling analysis module is used to analyze the geological conditions of the Xima River mining area, and the research on the rock bridge movement, deformation, and fracture evolution process and rock mass seepage characteristics in the Xima River mining area under the filling mining mode is carried out. The main conclusions are as follows:

(1) The volume of the plastic zone and the vertical displacement of monitoring points suddenly increase in the rock bridge area during mining 10 m and −150 m sections, and the rock mass may be damaged in a large area.

(2) The disturbance of ore body mining has not had a great adverse effect on the stability of the rock mass at the top of the F2 fault. The distribution of the rock mass destruction area caused by mining is limited to the local extent. From a holistic point of view, the damage zone was not fully penetrated through the stope-rock bridge-Xima River.

(3) The deformation and plastic damage of mining rock mass lead to increased permeability of rock mass. Isolines of pore water pressure in the stope roof tend to spread in the direction of faults. However, after the seepage field is basically stable, there is still no through drainage channel from surface water to the stope. Thus, it can be seen that the river does not change its course after the filling mining method which has certain safety and reliability.

Data Availability

All data generated or analyzed during this study are included within this article.

Conflicts of Interest

The authors declare that they have no conflicts of interest.

Acknowledgments

This research was funded by the National Natural Science Foundation of China (51874112 and 51774107) and the Open Research Fund Program of State Engineering Laboratory of Highway Maintenance Technology, Changsha University of Science and Technology (kfj170108). All financial support is gratefully acknowledged.

References

[1] Y. Lu and L. Wang, "Numerical simulation of mining-induced fracture evolution and water flow in coal seam floor above a confissned aquifer," *Computers and Geotechnics*, vol. 67, pp. 157–171, 2015.

[2] H. Liu and J. Xiang, "Kernel regression residual decomposition-based synchroextracting transform to detect faults in mechanical systems," *ISA Transactions*, vol. 87, 2019.

[3] H. Liu and J. Xiang, "Autoregressive model-enhanced variational mode decomposition for mechanical fault detection," *IET Science, Measurement & Technology*, vol. 13, no. 6, pp. 843–851, 2019.

[4] H. Liu and J. Xiang, "A strategy using variational mode decomposition, L-kurtosis and minimum entropy deconvolution to detect mechanical faults," *IEEE Access*, vol. 7, pp. 70564–70573, 2019.

[5] H. Liu and J. Xiang, "Kernel regression residual signal-based improved intrinsic time-scale decomposition for mechanical fault detection," *Measurement Science and Technology*, vol. 30, no. 1, Article ID 015107, 2018.

[6] T.-H. Yang, C. A. Tang, W. Zhu, and Q. Y. Feng, "Coupling analysis of seepage and stresses in rock failure process," *Chinese Journal of Geotechnical Engineering*, vol. 23, no. 4, pp. 489–493, 2001.

[7] T. Nie, H. Pu, and G. Liu, "Research on splitting failure model of fractured rock mass under the coupling effect of seepage-stress," *Journal of Mining & Safety Engineering*, vol. 32, no. 6, pp. 1026–1030, 2015.

[8] P.-S Zhang, W. Yan, and W.-Q. Zhang, "Mechanism of water inrush due to damage of floor and fault activation induced by mining coal seam with fault defects under fluid-solid coupling mode," *Chinese Journal of Geotechnical Engineering*, vol. 38, no. 5, pp. 877–889, 2016.

[9] Li.-P. Li, S.-C. Li, and S.-S. Shi, "Multi-field coupling mechanism of seepage damage for the water lnrush channel formation process of coal mine," *Journal of Mining & Safety Engineering*, vol. 29, no. 2, pp. 232–238, 2012.

[10] Y.-L. Lu, *Hydro-mechanical Modeling of Fracturing Evolution in Rocks and Mechanism of Water-Inrush from Coal Seam floor*, China University of Mining and Technology, Xuzhou, China, 2013.

[11] G.-L. Bai, "Fluid-Solid Coupling model of equivalent continuous mediumin overburden rock based on FLAC^{3D} and its a pplication," *Journal of Mining & Safety Engineering*, vol. 27, no. 1, pp. 110–114, 2010.

[12] D.-X. Yao and H.-F. Lu, "Seepage field-strain field coupling analysis for rock masses of coal seam floor during mining above a confinged aquifer," *Chinese Journal of Rock Mechanics and Engineering*, vol. 31, no. 1, pp. 2738–2744, 2012.

[13] J. A. Wang and H. D. Park, "Fluid permeability of sedimentary rocks in a complete stress-strain process," *Engineering Geology*, vol. 63, no. 3-4, pp. 291–300, 2002.

[14] M. D. Zoback and J. D. Byerlee, "The effect of microcrack dilatancy on the permeability of Westerly Granite," *Journal of Geophysical Research*, vol. 80, pp. 752–755, 1975.

[15] W. C. Zhu and C. H. Wei, "Numerical simulation on mining-induced water inrushes related to geologic structures using a damage-based hydromechanical model," *Environmental Earth Sciences*, vol. 62, no. 1, pp. 43–54, 2011.

[16] Y. Zhao and Q. Peng, "Fluid–solid coupling analysis of rock pillar stability for concealed karst cave ahead of a roadway based on catastrophic theory," *International Journal of Mining Science and Technology*, vol. 24, no. 6, pp. 737–745, 2014.

[17] E. Z. Lajtai, "Strength of discontinuous rocks in direct shear," *Géotechnique*, vol. 19, no. 2, pp. 218–233, 1969.

[18] Y.-M. Liu and C.-C. Xia, "Weakening mechanism of mechanical behaviors and failure models of rock mass containing discontinuous joints under direct shear condition," *Rock and Soil Mechanics*, vol. 31, no. 3, pp. 695–701, 2010.

[19] X.-G. Wang, Z.-X. Jia, Z.-Y. Chen, and Y. Xu, "Determination of discontinuity persistent ratio by Monte-Carlo simulation and dynamic programming," *Engineering Geology*, vol. 203, pp. 83–98, 2016.

[20] Z.-Q. Zhang, L. I. Ning, and F.-F. Chen, "Review and status of research on failure mode of nonpenetrative fractured rock mass," *Chinese Journal of Rock Mechanics and Engineering*, vol. 28, no. 9, p. 1945, 2009.

[21] R. H. C. Wong and K. T. Chau, "Crack coalescence in a rock-like material containing two cracks," *International Journal of Rock Mechanics and Mining Sciences*, vol. 35, no. 2, pp. 147–164, 1998.

[22] H. Wang and X.-D. Sun, "Simulation of fluid-solid interaction effect in rich water tunnel based on FLAC-3D," *Journal of Liaoning Technical University (Natural Science)*, vol. 4, pp. 468–473, 2015.

[23] T. H. Yang, C. A. Tang, L. C. Li et al., "Study on the evolution law of permeability in the fracture process of heterogeneous rocks," *Chinese Journal of Rock Mechanics and Engineering*, vol. 23, no. 5, pp. 758–762, 2004.

[24] L. C. Li, T. H. Yang, C. A. Tang et al., "Coupling analysis of rock hydraulic fracturing process," *Chinese Journal of Rock Mechanics and Engineering*, vol. 22, no. 7, p. 1060, 2003.

[25] J. R. Booker and J. C. Small, "An investigation of the stability of numerical solutions of Biot's equations of consolidation," *International Journal of Solids and Structures*, vol. 11, no. 7-8, pp. 907–917, 1975.

[26] F. J. Gaspar, F. J. Lisbona, and P. N. Vabishchevich, "A finite difference analysis of Biot's consolidation model," *Applied Numerical Mathematics*, vol. 44, no. 4, pp. 487–506, 2003.

[27] W. Song, J. Xiang, Y. Zhong et al., "A simulation-based method to detect mechanical parameters of I-beams and hollow cylinders," *Journal of Testing and Evaluation*, vol. 48, no. 6, 2020.

[28] W. Song, Y. Zhong, and J. Xiang, "Mechanical parameters identification for laminated composites based on the impulse excitation technique," *Composite Structures*, vol. 162, pp. 255–260, 2017.

[29] W. Song, Y. Zhong, and J. Xiang, "Mechanical parameters detection in stepped shafts using the FEM based IET," *Smart Structures & Systems*, vol. 20, no. 4, pp. 473–481, 2017.

[30] W. Song, Y. Zhong, and J. Xiang, "A simulation model based fault diagnosis method for bearings," *Journal of Intelligent & Fuzzy Systems*, vol. 34, pp. 3857–3867, 2018.